



Cite this: *Environ. Sci.: Nano*, 2023, 10, 424

Received 17th May 2022,
Accepted 3rd December 2022

DOI: 10.1039/d2en00469k

rsc.li/es-nano

Nanoparticles (NPs) interact within organisms *via* various biochemical interactions which can bring benefits to society. Classically, fate/distribution of substances is assessed *via* phase (octanol–water) based partitioning. A decade ago, Praetorius famously stated that phase-based partitioning for NPs is “a road to nowhere”. While (*in vivo*) experiments are cumbersome, reliable partitioning values are of utmost importance given a wealth of medicinal/toxicological and environmental exposure assessments. In this communication, we describe calculus for distribution in human tissues. We applied surface free energy components for NPs, cell membranes/vesicles, plasma and protein describing (van de Waals and Lewis acid–base) interactions amongst tissue and blood constituents. We considered neutral and charged NPs, and various tissues for statistical evaluation. Comparison to experiments showed that predictions are acceptable ($R^2 \geq 0.7$). Depending on surface functionality, phagocyte-rich and cancerous tissues accumulate NPs distinctly from ‘normal’ tissue, *via e.g.*, receptor (lectin/cadherin) binding. Our modeling study aids and supplements experiments to quantify the interactions, tissues concentrations and transport of NPs with(in) organs, to unravel mechanisms of human exposures. It provides a reference for partitioning to benchmark upcoming medical applications (*e.g.*, PBPK) and human/ecological risk assessments, enabling experimentalists more efficient monitoring, data interpretation, and reduces cost/time-intensive medicinal and toxicological campaigns.

1. Introduction

Nanoparticles (NPs)^{1,2} have a wide range of applications in chemical industry and in medicine.^{3,4} NPs are, *e.g.*, used therapeutically to target tumor cells. NPs however, also come with environmental risks^{5,6} depending on non-targeted

Nanoparticles in bodily tissues: predicting their equilibrium distributions

Tom M. Nolte, * Bingqing Lu and A. Jan Hendriks

Environmental significance

Current study in our research group deals with the prediction of distribution of nanoparticles in humans. This is crucial, but not adequately covered by current fate models. In this study surface-driven models were developed capable of predicting partitioning of structurally diverse nanoparticles. The developed models can be used to predict distribution in various tissues. The methods developed in our study are the first of its kind that allow for robust predictions that were not possible previously. We believe *Environmental Science: Nano* readers will benefit from the results outlined in this study as it aids their further research and policy decisions.

biochemical interactions.^{7,8} As NPs come in different materials and sizes, quantifying the impact of surface coating⁹/functionalization on NPs cellular transport has important implications in toxicology.

For decades, fate and accumulation of small organic compounds have been benchmarked using phase-behavior/partitioning.¹⁰ Oil–water^{11,12} and octanol–water partition coefficient (K_{ow}) have been used to predict NP accumulation/transformation in environments^{13,14} and organisms.^{10,15} However, NPs interact with bio-membrane surfaces,¹⁶ preventing dispersion.^{17,18} Interactions between NPs and biological matrices are difficult to characterize due to adsorption and (irreversible) agglomeration.

Pauli, markedly said, “God made the bulk; the surface was invented by the devil”.¹⁹ In a bulk phase, elements are surrounded by other similar elements. Surface elements interact either with elements from the same surface, or with elements located just below, above or beyond it. Therefore, properties of a phase and its energies differ depending upon location, making phase-partitioning inadequate to describe exposure. As NP interactions are surface-driven, Praetorius stated that “assessing NP fate *via* K_{ow} is a road to nowhere”.¹⁷

Fully empirical (*i.e.*, ‘black box’)²⁰ methods, evaluate cellular equilibria of NPs without regard for mechanism and have confined applicability due to lack of understanding. Instead, mechanistic insights are needed to describe NP-biological interactions semi-empirically. Current semi-

Department of Environmental Science, Institute for Biological and Environmental Sciences, Radboud University Nijmegen, 6500, GLNijmegen, The Netherlands.
E-mail: tom.m.nolte@gmail.com



empirical methods^{21,22} apply mechanisms but still have limited applicability to other exposure regimes.

Interaction with tissue components is at the basis of (NP) accumulation.^{23,24} Transport of NPs in(to) cells²⁵ depend on uptake pathway, possible *via* passive diffusion into/through the cytoplasm, adhesion to endoplasmic reticulum²⁶ or Golgi apparatus²⁷ to be encapsulated by membranes and vesicles,^{28–30} (*e.g.*, non-endocytic pathways for red blood cells³¹). NP can agglomerate in vesicles, to be excreted by cells.²⁹ NPs transport and accumulation (agglomeration) in/to lysosomes¹⁷ enables acid-catalyzed degradation,^{7,30,32,33} altering their surfaces.³⁴

Transport by vesicles³⁵ drives NP exo/endocytosis. Upon cytosol, cell membranes and vesicles deform to fuse and release/trap NPs.³⁶ Therefore, past research predicted transport based on membrane energies like crossing, deformation,^{37,38} encapsulation and combination.³⁹ Recent work⁴⁰ linked NP properties to traits of cells to assess interaction energy and predict cellular uptake and elimination. Properties of NPs, *e.g.*, charge (density⁴¹) and cell traits influence NP transport, but it remains difficult to characterize binding to vesicles. Identifying the probability/frequency of binding and transport⁴² enable assessing NP exposure.

Relationships between surface physico-chemical properties and cell behavior at the interface have been hypothesized.^{43–46} We specify this hypothesis by considering NP properties and tissue/cells traits to assess partitioning in organs, Fig. 1. In this communication, we quantify exposure by using interaction energies between NPs and membranes. We consider the fraction/frequency of NPs bound/encapsulated by/in organ(elles). We focus on polar (Lewis

acid–base) and Van de Waals forces. We assessed our model with experimental data for various tissues and explored the effect of NP properties on partitioning.

2. Methods

2.1. Tissue compositions

Tissue partitioning (K) is affected by the amount of membrane in a cell, and how many cells of a type an organ tissue contains. *E.g.*, cancerous cells express enhanced intracellular signaling *via* vesicles.^{48–52} As the concentration of cells and their membranes is in excess to NP concentration, we take that sorption is linear in NP concentration, and that K is a summation function over Boltzmann partitioning ($e^{-\Delta G_i/RT}$) among cell types (i), weighted by their proportion in the tissue:

$$K_{\text{tissue/blood}} = a \cdot \sum_i \left(\frac{[i]}{[\text{tot}_i]} \cdot e^{-\frac{\Delta G_{\text{membr}(i)/\text{water}}}{RT}} \right) + b \quad (1)$$

We take proportions of cell types from Table 1. We calculate binding energy changes ΔG_i from surface energies γ , section 2.3. Apart from membranes, proteins influence distribution of NPs. We take serum protein concentration independent of tissue type (equal among capillary bloods), and describe its influence in section 2.2. Knowing how much water organs contain, we extrapolate $e^{-\Delta G(\text{tissue/water})/RT}$ to $e^{-\Delta G(\text{organ/water})/RT}$, Table 1.

2.2. Membrane–protein–water partitioning

We calculate K_i *via* Boltzmann, *via* ΔG : values for free energy of binding. Fig. 1 depicts the influence of G

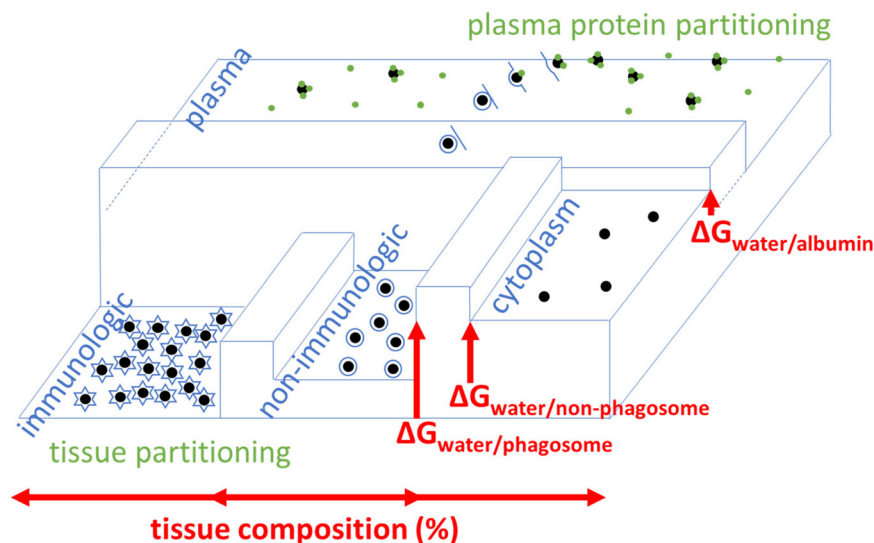


Fig. 1 Example distribution of NPs throughout/around tissues, influenced by energy G . Plasma = extracellular serum (saline water + protein).

Difference between dividing beams (barriers) are $\Delta G = \Delta G_{\text{on}}^{\ddagger} - \Delta G_{\text{off}}^{\ddagger}$, *i.e.*, $K = \frac{k_{\text{on}}}{k_{\text{off}}}$ denotes equilibrium which is attained after long-term exposure.

Intracellular vesicle-free NPs exist.⁴⁷ Low G means high NP concentration: $[\text{NP}]_i/[\text{NP}]_{\text{total}} = e^{-\Delta G_{\text{np-}i}/RT}$, depending on properties, accumulation in phagocytes/lysosomes.



Table 1 Simple representative composition (%) of healthy human organ tissues by generic celltype. Colors denote dominant contribution to energy (red = hydrophobic, blue = Lewis basic, green = Lewis acidic). We combined compositions with surface energy data (Table 2). Membrane types have varying degrees of immunological (Fig. 1) relevance^{53–70}

Membrane cell type i ^a	Liver	Bone; ^b spine	Skin	Spleen ^e	Adipos e	Tumor	Mucus	Blood	Lymph	Brain barrier ^d testis barrier	Lung; kidney; heart
Keratinocytes, %	0	0	59	0	0	0	0	0	0	0	0
Epith/endoth, %	5	1	40	5	0	0		0	0	100	99
Hepatocytes, %	70	0	0	0	0	0	0	0	0	0	0
Osteocytes, %	0	98	0	0	0	0	0	0	0	0	0
Phagocytes, ^c %	25	1	1	25	0	0	0	0.1	100	0	1
Lipocytes, %	0	0	0	0	100	0	0	0		0	0
Cancerous, %	0	0	0	0	0	100	0	0	0	0	0
Erythrocytes, %	0	0	0	70	0	0	0	99.9	0	0	0
Mucous cell, %	0	0	0	0	0	0	100	0	0	0	0
Total, %	100	100	100	100	100	100	100	100	100	100	100
Water, % (ref. 53)	72	31; 69	64	75	21	80	98	90	96	70	83; 82; 75
References	54–61	61–64	61	61, 65–68	—	—	69	61, 70	61	—	61

^a Representative functional cell; ^b excluding bone marrow; ^c assuming the majority of immunological cells is phagocytotic, ^d BBB consists of tightly packed endothelial cells. ^e White pulp (25% of splenic tissue) structurally similar to lymph.⁷¹

(vertical) across different surfaces/compartments (horizontal). The lower G , the higher the partitioning therein/on. The ability of NPs to partition onto membranes depend on their bio-availability, *i.e.*, interaction with endemic serum proteins,^{46,72,73} Fig. 1. We define partitioning of NPs between water (w) and membranes (m) as function of serum plasma protein coating in two additive terms:

$$e^{\frac{-\Delta G_{\text{membr}(i)/\text{water}}}{RT}} = \frac{e^{-\Delta G_{\text{water} \rightarrow \text{membr}(\text{serum})}/RT}}{(1 + \alpha \cdot e^{-\Delta G_{\text{serum} \rightarrow \text{water}(\text{NP})}/RT})} + \frac{e^{-\Delta G_{\text{water} \rightarrow \text{membr}(\text{NP})}/RT}}{(1 + \alpha \cdot e^{-\Delta G_{\text{water} \rightarrow \text{serum}(\text{NP})}/RT})} \quad (2)$$

where we take that a NP is either covered or uncovered by serum proteins (p), analogous to small organic molecules. α is a dimensionless frequency of NP-encounters, proportional to plasma protein amount (7%); inversely proportional to the NPs (surface area) acting as a plasma protein scavenger, $\alpha = \frac{0.07}{\left(\frac{[\text{NP}]}{[\text{serum}]}\right) + 1}$. RT is gas constant; temp.

Serum contains 60–80 g L⁻¹ plasma protein (35–50 g L⁻¹ albumin), with MW of ~150 kg mol⁻¹, thus (70/

150000) $\times 6.02 \times 10^{23} = 2.8 \times 10^{20}$ proteins per L (size $d_{\text{serum}} = 6$ nm), of which (1000/(6 \times 6) =) 28 can adsorb on 1000 nm² NP surface. Thus, protein concentration is in excess to NPs dosing concentration [NP] in any practical scenario (10⁶–10¹² NPs L⁻¹ (ref. 74)). We thus disregard NP homo-/heteroaggregation/agglomeration, taking $\alpha = 0.07$.

2.3. Free energy changes

We obtained different binding free energy changes ΔG via:

$$\begin{aligned} \Delta G_{\text{water} \rightarrow \text{membrane}(\text{serum})} &= A \cdot (\gamma_{\text{serum-plasma-membr}}^{\text{AB}} + \gamma_{\text{serum-plasma-membr}}^{\text{LW}}) \\ \Delta G_{\text{water} \rightarrow \text{membrane}(\text{NP})} &= A \cdot (\gamma_{\text{NP-plasma-membr}}^{\text{AB}} + \gamma_{\text{NP-plasma-membr}}^{\text{LW}}) \\ \Delta G_{\text{water} \rightarrow \text{serum}(\text{NP})} &= A \cdot (\gamma_{\text{NP-plasma-protein}}^{\text{AB}} + \gamma_{\text{NP-plasma-serum}}^{\text{LW}}) \\ \Delta G_{\text{serum} \rightarrow \text{water}(\text{NP})} &= -A \cdot (\gamma_{\text{NP-plasma-serum}}^{\text{AB}} + \gamma_{\text{NP-plasma-serum}}^{\text{LW}}) \quad (3) \end{aligned}$$

In ‘classical phase partitioning’ (for small organic compounds) A is the solvent accessible molecular surface



area. NP partitioning is geometry-driven;⁷⁵ we assume only partial wrapping of surface area (*e.g.*, bending/deformation negligible to AB/LW forces or compensated by receptor–ligand binding⁷⁶) estimating the interaction area (m^2) A from molar volume⁷⁷ (here, the ethylene glycol monomer of PEG). We involved Vande Waals (LW)/polar Lewis acid–base (AB) forces^{40,78} taking distances in equilibrium by born repulsion, 0.157 nm.⁷⁸

We calculated γ^{AB} and γ^{LW} ($mJ\ m^{-2}$) from effective surface energy components γ^{LW} , γ^+ and γ^- (electron acceptor and donor) for each species: NPs, membranes, serum plasma protein and water; details in ref. 78 and 79, substantiated by multiple cell lines (macrophage, endothelial cancer, fibroblast, *etc.*).^{80,81} We take for $\gamma_{protein}^+$, $\gamma_{protein}^-$, $\gamma_{protein}^{LW}$ of serum protein 0.002, 20, and 41 $mJ\ m^{-2}$, taken to resemble dry albumin at pH 7,^{79,82} and for γ_{plasma}^+ , γ_{plasma}^- , γ_{plasma}^{LW} of plasma 25.5, 25.5 and 21.8, $mJ\ m^{-2}$, taken to resemble water. For NP γ_{NP}^+ , γ_{NP}^- , γ_{NP}^{LW} we took 0, 45, and 43 $mJ\ m^{-2}$, taken to be polyethylene glycol.

2.4. Cell membrane types

While carbohydrate contents in membrane surfaces do not (greatly) differ between cell types,^{83–87} differentiation involves glycosylation:^{88–90} phagocyte have glycosylated protein receptors (lectins^{90,91}) with binding motifs specific to (β -) glucan-chitin copolymers^{92–94} recognizing foreign particles. Liver (Kupffer)^{92,95,96} and cancer cell^{97,98} membranes are lectin-rich. Immunological (mucus/phagocytic/cancerous)

cells have enhanced metabolism over ‘tranquil’/‘sluggish’, *e.g.*, endothelial cells.^{7,81,99,100}

Via abnormal metabolism cancer cells produce *e.g.*, lactate acidifying tissues,¹⁰¹ affecting bio-adsorption.^{102,103} Metastatic cancer cells migrate/proliferate to tissues *via* the blood,^{104,105} depending on hydrophilicity (*i.e.*, γ^{AB}). Cells contain many surfaces: Golgi apparatus/vesicles/lysosomes/endoplasmic reticulum. Liver macrophages internalize NPs^{106–108} and entail acid-rich lysosomes, attacking particles.^{109,110} pH can alter/affect surface activity, tension (γ)¹¹¹ and ‘biocollisions’.¹¹²

Membranes thereby differ in characteristic ‘surface acidity’,¹¹³ analogous to pK_a /pH functionalities among organic compounds (pK_a 's on surfaces).¹¹⁴ We characterize cell membrane type by energy of surfaces γ . Adipocytes contain more lipid (with specific γ).^{85,115} Table 2 lists $\gamma_{membrane}^+$, $\gamma_{membrane}^-$, $\gamma_{membrane}^{LW}$ values that we used to effectuate aforementioned factors, substantiated by relationships between phagocytosis/contact angle (*i.e.*, γ).⁴³

2.5. Testing using experimental tissue partitioning.

We evaluate accuracies of K from eqn (1)–(3) by comparison with experimentally-derived K from *in vivo* concentration data^{133,134} (open literature). We neglect biotransformation, and disregard elimination *via* faeces/urine. We focus on large exposure times t , *e.g.*, months,¹³³ so organs continuously take in/eliminate NPs (4, 13, 100 nm, coated with PEG) with equal rates. By analogy, barriers in Fig. 1 are sufficiently low. Then, dividing uptake and elimination gives K for organ tissues:

Table 2 Energy components of membrane surfaces in cell types ($mJ\ m^{-2}$). Ranges are variabilities across exp. setups. Colors denote dominant contribution to γ (red = hydrophobic, blue = basic polar, green = acidic polar). Octanol is a reference to phase partitioning^{44,116–131}

Membrane biomaterial type i	$\gamma_{membrane}^{LW}$	$\gamma_{membrane}^+$	$\gamma_{membrane}^-$	References
Keratinocyte ^a	32–36	0.0–1.3	7.5–14.5	116, 117
Epith/endoth ^b	37.6	0.00–1.05	59.6–76.7	118, 119
Hepatocyte ^c	39	0.00–1.05	54	120
Osteocyte ^d	42	0.2–0.3	39.1–60.6	121–124
Phagocyte ^{e,f}	28–30	5.3–7.7	18–23	44
Lipocyte	24.0–27.1	0	0	125–127
Cancerous ^{f,g}	36.0	1.23–1.70	50.9–53.7	118
Erythrocyte	35.2	0.01	46.2	128
Mucin/mucus	37.26/6.92	3.19/49.17	9.55/7.84	129, 130
Octanol	27.5	0	18.0	131

^a Values represent untreated keratinous skin, keratin <85% of differentiated keratinocytes.¹³² ^b Human endothelial cellline HUVEC. ^c Values unknown, γ^{LW} taken for a generic cell,^{78,80} γ^+ taken as range for non-immune cells, γ^- taken corresponding to maximum binding.¹²⁰ ^d For bone/osteocytes, membranes surface reflects hydroxyapatite, values represent untreated (hydrophilic) hydroxyapatite (>70% crystalline) and collagen. ^e Phagocytic cell lines THP-1, HL-60. ^f Local tissue/organelle pH enhances γ : linear/exponential extrapolations^{82,102} imply $\gamma^+ = 1.2$ –6.0 $mJ\ m^{-2}$, substantiating values reported. ^g Breast cancer cell line MCF-7.



$$\frac{k_{\text{in}}}{k_{\text{out}}} \cdot (1 - e^{-k_{\text{out}} \cdot t}) = \frac{[\text{NP}]_{\text{organ}}}{[\text{NP}]_{\text{blood}}} = K_{\text{tissue/blood}} \quad (4)$$

assuming that experiments reflect equilibrium. Section 4.2–4.4 discusses accuracy of the assumption.

3. Results

3.1. Interaction between NPs, membranes and serum

Table 2 shows energies for interaction between PEG-NPs and membrane biomaterial membrane surfaces (γ and ΔG). Interaction energies are either positive or negative. The larger the hydrophobicity and Lewis acidic character of the membrane, the more negative the energy values for interaction. The ΔG did not differ between differently sized PEG-NPs (4–100 nm) as the PEG coating groups are similarly sized.

The ΔG_{NP} range from -4.4 to $+5.1$ kJ mol^{-1} , which is an energy range of 9.5 kJ mol^{-1} . If $\Delta G_{\text{albumin}}$ were taken into account also, the summed ΔG is a range of -11.5 to $+7.8$ kJ mol^{-1} . This shows that albumin has a differentiating effect on cell type. Based on these values, *via* eqn (1)–(3), ratios were calculated for partitioning of PEG-NPs between serum and membranes. Predicted K was highest for non-polar lipocyte surfaces, and lowest for endothelial/epithelial cells. Again, the larger the hydrophobicity/Lewis acidic character of the membrane surface, the larger the predicted K .

3.2. Partitioning of NPs in organ tissues

Experimentally derived (eqn (4)) $K_{\text{tissue/blood}}$ for PEG-NPs range from 0.044 to 2600;¹³³ these K 's are independent of time within 7 days to 6 months. Other data for starch/dextran coated NPs¹³⁵ and eqn (4) imply a 3 day apparent tissue/blood/ K is ≥ 7 for phagocyte-rich tissues (*e.g.*, liver/spleen); for phagocyte-poorer tissues, $K_{\text{tissue/blood}} \geq 0.3$.¹³⁵ These values appear low compared to longer exposure times >7 days–6 months. This indicates absence of equilibrium or steady state. We did not see a statistically significant effect of NP size on the K_{exp} ,¹³³ Fig. 1. Surface functionality does influence partitioning, with 6 day $K_{\text{liver/blood}} > K_{\text{spleen/blood}}$ for cationic CTAB-NPs, but $K_{\text{liver/blood}} < K_{\text{spleen/blood}}$ for neutral PEG-NPs.¹³⁴

3.3. Prediction of NP partitioning

Fig. 2 depicts predicted K , eqn (1)–(3) and experimentally derived K (eqn (4)) for PEG-NP partitioning in different organ tissues, with reference to blood ($K_{\text{tissue/blood}}$). For 4 nm PEG-NPs, the Pearson correlation coefficient $R^2 = 0.69$ and $p = 0.0004$ (2SD). For 13 nm, $R^2 = 0.75$, $p = 0.0001$ (2SD) and for 100 nm $R^2 = 0.70$, $p = 0.0004$ (2SD). For 4, 13 and 100 nm grouped together, $R^2 = 0.68$, $p < 0.00001$ (2SD). The p values of these four linear regressions are all lower than 0.05 (SD), denoting statistically significant relationships. R^2 values are all higher than 0.6, which is often considered the minimally

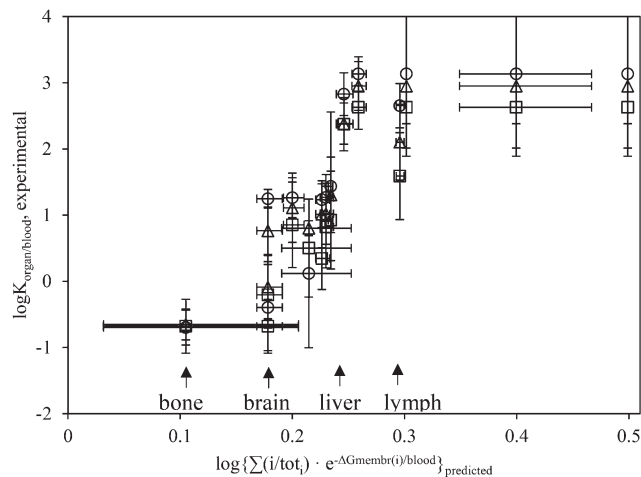


Fig. 2 Predicted (x -axis, eqn (1)–(3)) vs. experiment-derived partitioning between organ tissue (Table 1) and blood of PEG-NPs (Cho *et al.*¹³³ data, $N = 42$, eqn (4)). Circle $\circ = 4$ nm, triangle $\Delta = 13$ nm, square $\square = 100$ nm. Variance between same symbols due to difference in organ tissue composition (Table 1). Adipose tissue ($\log K_{\text{pred}} = 1.3$) shown as 0.5. Horizontal error bars propagate variabilities in γ^{membrane} (Table 2); vertical error bars are 1SD based on 4 datapoints. ΔG in 2.303 RT.

accepted prediction precision for (environmental) risk assessment.¹³⁶

The slope a of the linear regression (*i.e.*, $\log K_{\text{organ/blood,exp}} = a \cdot \log K_{\text{pred}} + b$) is approximately 15 ± 3 (2SD), significantly larger than 1. The offset b is -2 ± 1 (2SD). Regression fits (R^2) were slightly higher for a log-logistic fit, as compared to a linear fit. As adipose tissue appears out of domain, it was not taken into account in regressions. Values for predicted K for partitioning of PEG-NPs from blood into skin and adipose tissue were relatively high, ≥ 0.4 . Values for K_{pred} and K_{exp} for bone and brain were lowest. We did not observe any apparent outliers. Though we took data in Fig. 2 from 1 literature source,¹³³ other sources^{134,137–139} show similar trends for PEG. eqn (1)–(3) correctly predict that albumin adsorption for cationic NPs is higher than for anionic NPs.¹³⁴

$$\log K_{\text{organ/blood,experimental}} = 15(\pm 3) \cdot \log \left\{ \sum (i/\text{tot}_i) \cdot e^{-\Delta G_{\text{membrane}(i)/\text{blood}}} \right\}_{\text{predicted}} - (2 \pm 1)$$

4. Discussion

4.1. Energy considerations

Eqn (1)–(3) have a mechanistic basis. High/low K can be explained by many experimental phenomena. Cationic NPs (high γ^+) are cleared from blood (hence, organs) faster than neutral or anionic NPs,¹³⁷ presumably *via* enhanced binding to serum protein (high γ^-). Eqn (3) predicts this, which constitutes a basis for tissue partitioning. Organs rich in phagocytes show enhanced K ; indeed, NPs accumulate in lymph nodes.¹⁴⁰ Instead of polar headgroups (AB interaction), NPs may interact with lipid tails (micelle-like



system, involving differing γ (ref. 126 and 141)), as enhancing concentrations in adipose tissues (Fig. 2).

Across tissues, ΔG ranges from -4.4 to $+5.1$ kJ mol^{-1} , a range of 9.5 kJ mol^{-1} , equal to around 5–10 hydrogen (H) bonds. H-bonds need to be broken in order for surface molecules to interact. This number, ~ 10 kJ mol^{-1} , was associated to the difference between active and passive uptake mechanisms:^{142,143} cells with high positive ΔG (Table 3) take up PEG-NPs passively; cells with lower ΔG also take up PEG-NPs actively. The number of PEG chains on the (4 nm) NP surface would be ~ 40 ,^{144–146} but a limited number need interact with biomembranes. Molecular initiating interaction events (MIE) between substance and biomolecule/system (e.g., ~ 7 kJ mol^{-1} (ref. 147)) lead to outcome pathways. The MIE involves a limited/single functional group on the NP surface.

Though (e.g., lung) tissue contains only $\sim 1\%$ phagocytes, these contain up to 83% of all (PEG) NPs in tissue.¹⁴⁸ This implies a NP macrophage/tissue partitioning $K = (100/[\text{pha}]) \cdot ([\text{NP}_{\text{tot}}]/[\text{NP}_{\text{pha}}] - 1)$, i.e. $(100/[1]) \cdot ([100]/[83] - 1) = 20$. This 20-fold enhancement matches higher receptor densities¹⁴⁹ and activities¹⁵⁰ of macrophages. Moving 1 mol of a substance across a 20-fold gradient at 25 °C is $\Delta G = (8.315 \text{ J mol}^{-1} \text{ K}^{-1}) \cdot (298 \text{ K}) \cdot \ln(20/1) = 7.4 \text{ kJ mol}^{-1}$.¹⁵¹ It is therefore unlikely that slope = 15, larger than 1 (Fig. 2), stems from inaccurate γ (eqn (1)–(3), Table 2). If our ΔG is fully precise and exact, slope (Fig. 2) should be 1 (according to Boltzmann). The difference between expected (1) and observed (~ 15) may relate (partially) to unanticipated wrapping/bending or (geometry)-specific ligand–receptor energies^{152–154} contributing to γ , not reflected by Table 2, which may refine K . After phagocytosis, a cell minimizes its surface tension (γ) by smoothening.¹⁵⁵

4.2. Cell signaling

Not the full NP surface area interacts with the biomembrane surface. Indeed, K_{exp} does not differ between NP sizes¹³³ (Fig. 2). Log-logistic fits are slightly better than linear fits between K_{exp} and K_{pred} (levelling off in Fig. 2), implying a crowding/shielding/saturation. This may refer to interaction area A (eqn (3)), which varies depending on strength of interaction (ΔG). ΔG depends on polymer size, but approaches (per monomer unit) zero at higher MW.¹⁵⁶ Chemical potential of an atom/molecule depends on its surrounding, larger on convex surfaces than on flat surfaces, in turn larger than under concaves.¹⁵⁷ While size/geometry can affect γ ,^{158,159} interaction with serum/cytoplasmic constituents and geometric restrictions may offset the effect. The slope (~ 15) is thus not a size-effect *per se*.

The slope (Fig. 2) may entail information on frequency, α in eqn (2) or i in eqn (1). Under steady state, it implies higher phagocytic activity. By analogy, in (eco)toxicology, $\text{IC}_{50}/\text{EC}_{50}$ values (in log-logistic curves) describe induction of biological response. Indeed, high (toxic) pressures instigate aggrupation of phagocytes (granuloma) at sites of NPs (increasing i/tot_i for phagocytes, eqn (1)). We assumed that one NP binds to/within one vesicle^{42,160} ignoring (intracellular) aggregation.³³ This is sometimes not true: spleen phagocytes cluster (bioconcentrate) PEG-NPs in lysosomes;¹³³ Kupffer macrophages engorge NP-aggregates.¹⁶¹ Aggregation changes the properties of the NP cluster.

A 10-fold increase in the average number of NPs per lysosome, implies an effective ‘bioconcentration factor’ of 10. Bioaccumulation (in organisms), rather, involves multiple uptake steps by different signaling pathways. Detecting bioactive substances enhances local internal

Table 3 Surface energies changes for adsorption interaction of albumin and PEG-NPs onto membranes biomaterials i , and for sorption of albumin onto PEG-NPs. Corresponding membrane–serum partitioning ratio K (eqn (2)) also shown. $\gamma_{\text{NP}}^{\text{water} \rightarrow \text{albumin}} = 4.2 \text{ mJ m}^{-2}$

Membrane biomaterials type i	$\gamma_{\text{albumin}}^{\text{water} \rightarrow \text{membrane}}$, mJ m^{-2}	$\gamma_{\text{NP}}^{\text{water} \rightarrow \text{membrane}}$, mJ m^{-2}	$\Delta G_{\text{albumin}}^{\text{water} \rightarrow \text{membrane}}$, kJ mol^{-1}	$\Delta G_{\text{NP}}^{\text{water} \rightarrow \text{membrane}}$, kJ mol^{-1}	Predicted K membrane/serum, eqn (1)–(3)
Keratinocyte	−26.3	−7.8	−3.2	−1.0	5.0
Epith/endoth	+21.9	+41.2	+2.7	+5.1	0.5
Hepatocyte	+12.5	+31.7	+1.5	+3.9	0.7
Osteocyte	+8.7	+28.7	+1.1	+3.5	0.9
Phagocyte	−10.6	+0.3	−1.3	0.0	2.6
Lipocyte	−57.7	−35.7	−7.1	−4.4	23.0
Cancerous	+12.7	+29.6	+1.6	+3.7	0.7
Erythrocyte	+7.4	+29.3	+0.9	+3.6	0.9
Mucus	−13.2	−21.5	−1.6	−2.7	4.7



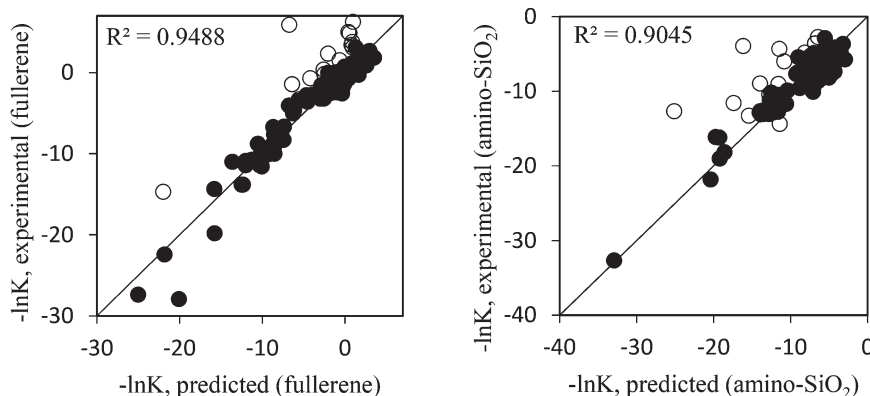


Fig. 3 Experimental vs. predicted partitioning for 155 biomolecules between water and fullerene C_{60} (left) and amino-functionalized SiO_2 NPs (right). Experimental values characterize partitioning of NPs onto (within) biomolecules and water. Data from ref. 215. Open symbols are (incompletely characterized mixtures of large) flexible molecules that minimize energy by molecular reorientation (oligonucleotides, small proteins). Interaction with C_{60} (γ_{LW} , γ^+ , $\gamma^- = 25, 2, 17 \text{ mJ m}^{-2}$) via polarization and electron donation; with (cationic) SiO_2-NH_3 (γ_{LW} , γ^+ , $\gamma^- = 0, 50, 0.1 \text{ mJ m}^{-2}$) via electron accepting.

concentrations.^{162–164} BAFs along (cell signaling^{94,165}) pathways may be ~ 100 times higher than BCF for the same substance.¹⁶⁶ Bioaccumulation K_{BAF} may be described as $K_{BCF} \cdot K_{BCF} \cdot K_{BCF} \dots$ etc., involving multiple concentrating steps (after the MIE).

Such steps may involve Ca^{2+} , affecting lectin binding capacity,^{91,165,167} which γ (Table 2) not captures. Cancer cells lack Ca^{2+} -dependent cadherin^{168–170} enhancing repulsion. Saline solutions effectuate different γ than pure water^{75,129} (eqn (3)). Amine-binding is key to pathogen detection and immune response,^{171–174} with electron-acceptor/donor interactions central to lectin binding to chitin ($\gamma^{LW} = 41$, $\gamma^+ = 1.3$, $\gamma^- = 17.1 \text{ mJ m}^{-2}$ (ref. 175)) via the *N*-acetyl group.¹⁷⁶ Ca^{2+} complexation (bridging) affects its ΔG .^{177–180} This explains the high slope (Fig. 2) because Ca^{2+} is only relevant in those (*i.e.*, immunological) tissues.¹⁸¹ For phagocytes, a decrease by Ca^{2+} in $\Delta G_{NP}^{water \rightarrow membrane}$ from 0 (Table 3) by a representative -25 kJ mol^{-1} (ref. 182 and 183) increases predicted $\log K$ for *e.g.*, the liver to ~ 2.9 , agreeing with experiment (2.4–2.8, Fig. 2).

4.3. Tissue inhomogeneities

Stronger correlations may imply a more homogeneous tissues or uniform binding mechanism. Inhomogeneities (*e.g.*, layering) in tissues affect K (hence, R^2 , Fig. 2) via local increased exposures. Penetration of PEG-NPs through skin depends on hydration status.^{75,184,185} Mucus epithelial tissue (mouth/stomach) cells produce (*N*-)glycosylated proteins¹⁸⁶ protecting organisms by binding (trapping) foreign material.^{187,188} This explains marked accumulation of NPs in (Ca^{2+} -augmented) mucin (Table 3),^{189,190} having distinct γ (Table 1).

We cannot always assume the barriers in Fig. 1 are sufficiently low; inhibition of transport limits tissue partitioning.⁸¹ Macrophages (microglia) account for 10–15% of brain cells,¹⁹¹ and would readily take up NPs.¹⁹² However, the brain's blood vessels are lined with endothelial cells

wedged tightly together, creating a boundary. Likewise, microvascular endothelial cells form the blood–spinal cord barrier; Sertoli cells constitute the blood–testis barrier. Pores sizes of $\sim 5 \text{ nm}$ may complicate measuring a K in kidney.

We characterized each individual membrane surface (and serum protein) by a single γ set, implying that *e.g.*, vesicles share the characteristics of cell surfaces, which combine during cytolysis. γ_{membrane} characterizes weighted averages of membrane components: lipids, receptors/proteins, counterions, etc. However, generic description of γ may not apply. Inhomogeneity in tissues is apparent from *e.g.* markedly different γ for bile in the liver ($\gamma^{LW} = 23–26$, $\gamma^+ = 36–46$, $\gamma^- = 8–15 \text{ mJ m}^{-2}$,¹⁹³ and $\gamma^+ = 10–13$, $\gamma^- = 35–41$, $\gamma^{LW} = 25–27 \text{ mJ m}^{-2}$ (ref. 194)) and hydroxyapatite ($\gamma^{LW} = 2.2$, $\gamma^+ = 19.8$, $\gamma^- = 73.2 \text{ mJ m}^{-2}$ (ref. 195)), differing from Table 2. In reality, γ_{membrane} differs across cell membranes. Pending (experimental) data, implementing distributions of γ_{membrane} for inhomogeneous surfaces renders predictions more precise.

NP distribution depend on interaction with (intra) cellular/tissue compartments, other than in Table 1.^{196,197} A diversity of proteins in biological media^{198,199} may differentially functionalize NPs (and membranes) affecting γ , but was ignored. Tissue composition (Table 1) may be dependent on NP concentration, characterizable by healthy/affected tissues, in terms of phagocytes.²⁰⁰ Differences in body/organ weights and composition exist.^{163,201} We presume that inter-²⁰² and intraspecies⁸⁶ differences in lectin contribute to variance in NP distribution. Human physiology is not an exact science; assessments need customization. Standardization helps to benchmark exposures and tailor assessments.

4.4. Outlook and conclusion

Performance of eqn (1)–(3) is appreciable, $R^2 = 0.68$, and statistically significant $p < 0.00001$ (2SD). In comparison,



- 14 B. A. M. Bandowe, M. Bigalke, J. Kobza and W. Wilcke, Sources and fate of polycyclic aromatic compounds (PAHs, oxygenated PAHs and azaarenes) in forest soil profiles opposite of an aluminium plant, *Sci. Total Environ.*, 2018, **630**, 83–95.
- 15 Y. Zhang, X. J. Luo, L. Mo, J. P. Wu, B. X. Mai and Y. H. Peng, Bioaccumulation and translocation of polyhalogenated compounds in rice (*Oryza sativa* L.) planted in paddy soil collected from an electronic waste recycling site, South China, *Chemosphere*, 2015, **137**, 25–32.
- 16 E. Price and A. J. Gesquiere, An in vitro assay and artificial intelligence approach to determine rate constants of nanomaterial-cell interactions, *Sci. Rep.*, 2019, **9**, 1394.
- 17 A. Praetorius, N. Tufenkji, K. U. Goss, M. Scheringer, F. von der Kammer and M. Elimelech, The road to nowhere: equilibrium partition coefficients for nanoparticles, *Environ. Sci.: Nano*, 2014, **1**, 317–323.
- 18 M. Crane, R. D. Handy, J. Garrod and R. Owen, Ecotoxicity test methods and environmental hazard assessment for engineered nanoparticles, *Ecotoxicology*, 2008, **17**, 421–437.
- 19 W. Pauli, God made the bulk; surfaces were invented by the devil, As quoted in *Growth, Dissolution, and Pattern Formation in Geosystems*, ed. B. Jamtveit and P. Meakin, 1999, p. 291.
- 20 A. I. Khan, Q. Lu, D. Du, Y. H. Lin and P. Dutta, Quantification of kinetic rate constants for transcytosis of polymeric nanoparticle through blood-brain barrier, *Biochim. Biophys. Acta, Gen. Subj.*, 2018, **1862**, 2779–2787.
- 21 S. Ohta, S. Inasawa and Y. Yamaguchi, Real time observation and kinetic modeling of the cellular uptake and removal of silicon quantum dots, *Biomaterials*, 2012, **33**, 4639–4645.
- 22 W. B. Chen, D. Z. D'Argenio, A. Sipos, K. J. Kim and E. D. Crandall, Biokinetic modeling of nanoparticle interactions with lung alveolar epithelial cells: uptake, intracellular processing, and egress, *Am. J. Physiol. Regul. Integr. Comp. Physiol.*, 2021, **320**, R36–R43.
- 23 N. W. van den Brink, A. Jemec Kokalj, P. V. Silva, E. Lahive, K. Norrfors, M. Baccaro, Z. Khodaparast, S. Loureiro, D. Drobne, G. Cornelis, S. Lofts, R. D. Handy, C. Svendsen, D. Spurgeon and C. A. M. van Gestel, Tools and rules for modelling uptake and bioaccumulation of nanomaterials in invertebrate organisms, *Environ. Sci.: Nano*, 2019, **6**, 1985.
- 24 J. Mosquera, I. Garcia and L. M. Liz-Marzan, Cellular Uptake of Nanoparticles versus Small Molecules: A Matter of Size, *Acc. Chem. Res.*, 2018, **51**, 2305–2313.
- 25 P. Ruenraroengsak, P. Novak, D. Berhanu, A. J. Thorley, E. Valsami-Jones, J. Gorelik, Y. E. Korchev and T. D. Tetley, Respiratory epithelial cytotoxicity and membrane damage (holes) caused by amine-modified nanoparticles, *Nanotoxicology*, 2012, **6**, 94–108.
- 26 E. Frohlich, Cellular elimination of nanoparticles, *Environ. Toxicol. Pharmacol.*, 2016, **46**, 90–94.
- 27 E. Silva, L. Barreiros, M. A. Segundo, S. A. C. Lima and S. Reis, Cellular interactions of a lipid-based nanocarrier model with human keratinocytes: Unravelling transport mechanisms, *Acta Biomater.*, 2017, **53**, 439–449.
- 28 P. Nativo, I. A. Prior and M. Brust, Uptake and intracellular fate of surface-modified gold nanoparticles, *ACS Nano*, 2008, **2**, 1639–1644.
- 29 V. Marchesano, Y. Hernandez, W. Salvenmoser, A. Ambrosone, A. Tino, B. Hobmayer, J. M. de la Fuente and C. Tortiglione, Imaging Inward and Outward Trafficking of Gold Nanoparticles in Whole Animals, *ACS Nano*, 2013, **7**, 2431–2442.
- 30 H. E. Chung, D. H. Park, J. H. Choy and S. J. Choi, Intracellular trafficking pathway of layered double hydroxide nanoparticles in human cells: Size-dependent cellular delivery, *Appl. Clay Sci.*, 2012, **65–66**, 24–30.
- 31 M. Geiser, B. Rothen-Rutishauser, N. Kapp, S. Schurch, W. Kreyling, H. Schulz, M. Semmler, V. I. Hof, J. Heyder and P. Gehr, Ultrafine particles cross cellular membranes by nonphagocytic mechanisms in lungs and in cultured cells, *Environ. Health Perspect.*, 2005, **113**, 1555–1560.
- 32 X. W. Wang, Y. H. Qiu, M. Y. Wang, C. H. Zhang, T. S. Zhang, H. M. Zhou, W. X. Zhao, W. L. Zhao, G. M. Xia and R. G. Shao, Endocytosis and Organelle Targeting of Nanomedicines in Cancer Therapy, *Int. J. Nanomed.*, 2020, **15**, 9447–9467.
- 33 B. D. Chithrani and W. C. W. Chan, Elucidating the mechanism of cellular uptake and removal of protein-coated gold nanoparticles of different sizes and shapes, *Nano Lett.*, 2007, **7**, 1542–1550.
- 34 A. Sipos, K. J. Kim, R. H. Chow, P. Flodby, Z. Borok and E. D. Crandall, Alveolar epithelial cell processing of nanoparticles activates autophagy and lysosomal exocytosis, *Am. J. Physiol. Lung Cell. Mol. Physiol.*, 2018, **315**, L286–L300.
- 35 P. Foroozandeh and A. A. Aziz, Insight into Cellular Uptake and Intracellular Trafficking of Nanoparticles, *Nanoscale Res. Lett.*, 2018, **13**, 33.
- 36 H. Deng, P. Dutta and J. Liu, Stochastic modeling of nanoparticle internalization and expulsion through receptor-mediated transcytosis, *Nanoscale*, 2019, **11**, 11227–11235.
- 37 H. Y. Tang, H. F. Ye, H. W. Zhang and Y. G. Zheng, Aggregation of nanoparticles regulated by mechanical properties of nanoparticle-membrane system, *Nanotechnology*, 2018, **29**(40), 405102.
- 38 A. Dey, J. Stenberg, P. Dandekar and R. Jain, A combinatorial study of experimental analysis and mathematical modeling: How do chitosan nanoparticles deliver therapeutics into cells?, *Carbohydr. Polym.*, 2020, **229**, 115437.
- 39 V. P. Zhdanov, Interpretation of amperometric kinetics of content release during contacts of vesicles with a lipid membrane, *Eur. Biophys. J.*, 2017, **46**, 461–470.
- 40 B. Q. Lu, A. J. Hendriks and T. M. Nolte, A generic model based on the properties of nanoparticles and cells for predicting cellular uptake, *Colloids Surf., B*, 2022, **209**(1), 112155.



- 41 A. Bigdeli, M. R. Hormozi-Nezhad and H. Parastar, Using nano-QSAR to determine the most responsible factor(s) in gold nanoparticle exocytosis, *RSC Adv.*, 2015, **5**, 57030–57037.
- 42 P. Rees, J. W. Wills, M. R. Brown, C. M. Barnes and H. D. Summers, The origin of heterogeneous nanoparticle uptake by cells, *Nat. Commun.*, 2019, **10**, 2341.
- 43 J. Vitte, A. M. Benoliel, A. Pierres and P. Bongrand, Is there a predictable relationship between surface physical-chemical properties and cell behaviour at the interface?, *Eur. Cells Mater.*, 2004, **7**, 52–63.
- 44 J. Da Silva Domingues, Macrophage-mediated phagocytosis of bacteria adhering on biomaterial surfaces, *PhD*, University of Groningen, 2014, ch. III. Phagocytosis of bacteria adhering to a biomaterial surface in a surface thermodynamic perspective.
- 45 C. H. Achebe, S. Iweriolor and J. L. Chukwunneke, Surface Energetics Study and Determination of the Combined Negative Hamaker Coefficient for Hepatitis C Virus Infected Human Blood Cells, *J. Biomed. Sci. Eng.*, 2018, **11**, 307–319.
- 46 I. Lynch, A. Ahluwalia, D. Boraschi, H. J. Byrne, B. Fadeel, P. Gehr, A. C. Gutleb, M. Kendall and M. G. Papadopoulos, The bio-nano-interface in predicting nanoparticle fate and behaviour in living organisms: towards grouping and categorising nanomaterials and ensuring nanosafety by design, *BioNanoMat*, 2013, **14**, 195–216.
- 47 Y. Y. Liu, Q. Chang, Z. X. Sun, J. Liu, X. Y. Deng, Y. F. Liu, A. N. Cao and H. F. Wang, Fate of CdSe/ZnS quantum dots in cells: Endocytosis, translocation and exocytosis, *Colloids Surf., B*, 2021, **208**, 112140.
- 48 A. Becker, B. K. Thakur, J. M. Weiss, H. S. Kim, H. Peinado and D. Lyden, Extracellular Vesicles in Cancer: Cell-to-Cell Mediators of Metastasis, *Cancer Cell*, 2016, **30**, 836–848.
- 49 R. Szatanek and M. Baj-Krzyworzeka, CD44 and Tumor-Derived Extracellular Vesicles (TEVs). Possible Gateway to Cancer Metastasis, *Int. J. Mol. Sci.*, 2021, **22**(3), 1463.
- 50 E. M. Guerreiro, R. Ovstebo, B. Thiede, D. E. Costea, T. M. Soland and H. Kanli Galtung, Cancer cell line-specific protein profiles in extracellular vesicles identified by proteomics, *PLoS One*, 2020, **15**, e0238591.
- 51 W. Tian, N. Lei, J. Zhou, M. Chen, R. Guo, B. Qin, Y. Li and L. Chang, Extracellular vesicles in ovarian cancer chemoresistance, metastasis, and immune evasion, *Cell Death Dis.*, 2022, **13**, 64.
- 52 K. Wu, F. Xing, S. Y. Wu and K. Watabe, Extracellular vesicles as emerging targets in cancer: Recent development from bench to bedside, *Biochim. Biophys. Acta, Rev. Cancer*, 2017, **1868**, 538–563.
- 53 R. Pethig and D. B. Kell, The passive electrical properties of biological systems: their significance in physiology, biophysics and biotechnology, *Phys. Med. Biol.*, 1987, **32**, 933–970.
- 54 E. Pandey, A. S. Nour and E. N. Harris, Prominent Receptors of Liver Sinusoidal Endothelial Cells in Liver Homeostasis and Disease, *Front. Physiol.*, 2020, **11**, 873.
- 55 D. V. Haute and J. M. Berlin, Challenges in realizing selectivity for nanoparticle biodistribution and clearance: lessons from gold nanoparticles, *Ther. Delivery*, 2017, **8**, 763–774.
- 56 C. I. Colino, J. M. Lanao and C. Gutierrez-Millan, Targeting of Hepatic Macrophages by Therapeutic Nanoparticles, *Front. Immunol.*, 2020, **11**, 218.
- 57 M. Bilzer, F. Roggel and A. L. Gerbes, Role of Kupffer cells in host defense and liver disease, *Liver Int.*, 2006, **26**, 1175–1186.
- 58 L. Bouwens, M. Baekeland, R. De Zanger and E. Wisse, Quantitation, tissue distribution and proliferation kinetics of Kupffer cells in normal rat liver, *Hepatology*, 1986, **6**, 718–722.
- 59 A. K. Sohlenius-Sternbeck, Determination of the hepatocellularity number for human, dog, rabbit, rat and mouse livers from protein concentration measurements, *Toxicol. In Vitro*, 2006, **20**, 1582–1586.
- 60 Z. E. Wilson, A. Rostami-Hodjegan, J. L. Burn, A. Tooley, J. Boyle, S. W. Ellis and G. T. Tucker, Inter-individual variability in levels of human microsomal protein and hepatocellularity per gram of liver, *Br. J. Clin. Pharmacol.*, 2003, **56**, 433–440.
- 61 M. Aborig, P. R. V. Malik, S. Nambiar, P. Chelle, J. Darko, A. Mutsaers, A. N. Edginton, A. Fleck, E. Osei and S. Wettig, Biodistribution and Physiologically-Based Pharmacokinetic Modeling of Gold Nanoparticles in Mice with Interspecies Extrapolation, *Pharmaceutics*, 2019, **11**(4), 179.
- 62 Q. Gu, H. Yang and Q. Shi, Macrophages and bone inflammation, *J. Orthop. Translat.*, 2017, **10**, 86–93.
- 63 E. L. Orr, J. E. Aschenbrenner, L. X. Oakford, F. L. Jackson and N. C. Stanley, Changes in brain and spinal cord water content during recurrent encephalomyelitis in female lewis rats, *Mol. Chem. Neuropathol.*, 1994, **22**, 185.
- 64 A. V. Leonard, E. Thornton and R. Vink, NK1 Receptor Blockade Is Ineffective in Improving Outcome following a Balloon Compression Model of Spinal Cord Injury, *PLoS One*, 2014, **9**, e98364.
- 65 C. E. Pochedly, *Disorders of the Spleen: Pathophysiology and Management*, Informa Health Care, 1989, pp. 7–15, ISBN 0–8247–7933–9.
- 66 M. Gualdrón-Lopez, M. Diaz-Varela, H. Toda, I. Aparici-Herrera, L. Pedro-Cos, R. Lauzurica, M. V. G. Lacerda, M. A. Fernandez-Sanmartin, C. Fernandez-Becerra and H. A. Del Portillo, Multiparameter Flow Cytometry Analysis of the Human Spleen Applied to Studies of Plasma-Derived EVs From Plasmodium vivax Patients, *Front. Cell. Infect. Microbiol.*, 2021, **11**, 596104.
- 67 K. Lee, K. Jeoung, S. H. Kim, Y. B. Ji, H. Son, Y. Choi, Y. M. Huh, J. S. Suh and S. J. Oh, Measuring water contents in animal organ tissues using terahertz spectroscopic imaging, *Biomed. Opt. Express*, 2018, **9**, 1582–1589.
- 68 G. Attina, S. Triarico, A. Romano, P. Maurizi, S. Mastrangelo and A. Ruggiero, Role of Partial Splenectomy in Hematologic Childhood Disorders, *Pathogens*, 2021, **10**(11), 1436.



- 127 I. Yildirim, Surface Free Energy Characterization of Powders, *Doctor of Philosophy*, Virginia Polytechnic Institute and State University, 2001, ch. 1.
- 128 Z. Lin, D. Ba and C. M. Liu, Surface Energy and Work of Adhesion of Titania-related Materials, *Phys. Procedia*, 2012, **32**, 580–589.
- 129 M. Rillosi and G. Buckton, Modelling mucoadhesion by use of surface energy terms obtained by the Lewis acid-Lewis base approach, *Int. J. Pharm.*, 1995, **117**, 75–84.
- 130 A. Alhalaweh, A. Vilinska, E. Gavini, G. Rassu and S. P. Velaga, Surface thermodynamics of mucoadhesive dry powder formulation of zolmitriptan, *AAPS PharmSciTech*, 2011, **12**, 1186–1192.
- 131 C. J. van Oss, *Interfacial Forces in Aqueous Media*, Marcel Dekker, New York, 1994.
- 132 E. Fuchs, Keratins and the skin, *Annu. Rev. Cell Dev. Biol.*, 1995, **11**, 123–153.
- 133 W. S. Cho, M. Cho, J. Jeong, M. Choi, B. S. Han, H. S. Shin, J. Hong, B. H. Chung, J. Jeong and M. H. Cho, Size-dependent tissue kinetics of PEG-coated gold nanoparticles, *Toxicol. Appl. Pharmacol.*, 2010, **245**, 116–123.
- 134 D. P. Lankveld, R. G. Rayavarapu, P. Krystek, A. G. Oomen, H. W. Verharen, T. G. van Leeuwen, W. H. De Jong and S. Manohar, Blood clearance and tissue distribution of PEGylated and non-PEGylated gold nanorods after intravenous administration in rats, *Nanomedicine*, 2011, **6**, 339–349.
- 135 J. A. Tate, A. A. Petryk, A. J. Giustini and P. J. Hoopes, In vivo biodistribution of iron oxide nanoparticles: an overview, *Proc. SPIE*, 2011, **7901**, 790117.
- 136 A. Golbraikh and A. Tropsha, Predictive QSAR modeling based on diversity sampling of experimental datasets for the training and test set selection, *J. Comput.-Aided Mol. Des.*, 2002, **16**, 357–369.
- 137 X. Li, B. Wang, S. Zhou, W. Chen, H. Chen, S. Liang, L. Zheng, H. Yu, R. Chu, M. Wang, Z. Chai and W. Feng, Surface chemistry governs the sub-organ transfer, clearance and toxicity of functional gold nanoparticles in the liver and kidney, *J. Nanobiotechnol.*, 2020, **18**, 45.
- 138 T. Dubaj, K. Kozics, M. Sramkova, A. Manova, N. G. Bastus, O. H. Moriones, Y. Kohl, M. Dusinska, E. Runden-Pran, V. Puentes, A. Nelson, A. Gabelova and P. Simon, Pharmacokinetics of PEGylated Gold Nanoparticles: In Vitro-In Vivo Correlation, *Nanomaterials*, 2022, **12**(3), 511.
- 139 C. M. Lavelle, J. H. Bisesi, M. H. Hahn, K. J. Kroll, T. Sabo-Attwood and N. D. Denslow, Oral bioavailability and sex specific tissue partitioning of quantum dots in fathead minnows *Pimephales promelas*, *Environ. Sci.: Nano*, 2015, **2**, 583.
- 140 C. Kuroda, K. Ajima, K. Ueda, A. Sobajima, A. Sobajima, K. Yoshida, T. Kamanaka, J. Sasaki, H. Ishida, H. Haniu, M. Okamoto and K. Aoki, Isolated lymphatic vessel lumen perfusion system for assessing nanomaterial movements and nanomaterial-induced responses in lymphatic vessels, *Nano Today*, 2021, **36**, 101018.
- 141 H. J. Cho, S. C. Maroo and E. N. Wang, *Characterization of Lipid Membrane Properties for Tunable Electroporation*, ASME 2012 Third International Conference on Micro/Nanoscale Heat and Mass Transfer, 3–6 March 3, 2012, ASME, Atlanta, Georgia, 2012.
- 142 E. Canepa, S. Salassi, F. Simonelli, R. Ferrando, R. Rolandi, C. Lambruschini, F. Canepa, S. Dante, A. Relini and G. Rossi, Non-disruptive uptake of anionic and cationic gold nanoparticles in neutral zwitterionic membranes, *Sci. Rep.*, 2021, **11**, 1256.
- 143 A. Ghavami, E. van der Giessen and P. R. Onck, Energetics of Transport through the Nuclear Pore Complex, *PLoS One*, 2016, **11**, e014887.
- 144 L. Shi, J. Zhang, M. Zhao, S. Tang, X. Cheng, W. Zhang, W. Li, X. Liu, H. Peng and Q. Wang, Effects of polyethylene glycol on the surface of nanoparticles for targeted drug delivery, *Nanoscale*, 2021, **13**, 10748–10764.
- 145 X. Xia, M. Yang, Y. Wang, Y. Zheng, Q. Li, J. Chen and Y. Xia, Quantifying the coverage density of poly(ethylene glycol) chains on the surface of gold nanostructures, *ACS Nano*, 2012, **6**, 512–522.
- 146 J. Manson, D. Kumar, B. J. Meenan and D. Dixon, Polyethylene glycol functionalized gold nanoparticles: the influence of capping density on stability in various media, *Gold Bull.*, 2011, **44**, 99–105.
- 147 P. M. Paarakh, D. C. Sreeram, S. S. D and S. P. Ganapathy, In vitro cytotoxic and in silico activity of piperine isolated from Piper nigrum fruits Linn, *In Silico Pharmacol.*, 2015, **3**, 9.
- 148 M. Geiser, O. Quaile, A. Wenk, C. Wigge, S. Eigeldinger-Berthou, S. Hirn, M. Schaffler, C. Schleh, W. Moller, M. A. Mall and W. G. Kreyling, Cellular uptake and localization of inhaled gold nanoparticles in lungs of mice with chronic obstructive pulmonary disease, *Part. Fibre Toxicol.*, 2013, **10**, 19.
- 149 R. L. Griffith, G. T. Virella, H. C. Stevenson and M. F. Lopes-Virella, Low density lipoprotein metabolism by human macrophages activated with low density lipoprotein immune complexes, A possible mechanism of foam cell formation, *J. Exp. Med.*, 1988, **168**, 1041–1059.
- 150 N. Im, T. D. Yang, K. Park, J. Lee, J. Lee, Y. H. Kim, J. Lee, B. Kim, K. Jung, Y. Choi and S. Baek, Application of M1 macrophage as a live vector in delivering nanoparticles for in vivo photothermal treatment, *J. Adv. Res.*, 2021, **31**, 155–163.
- 151 A. L. Lehninger, D. L. Nelson and M. M. Cox, *Principles of Biochemistry*, Worth, New York, 2nd edn, 1993.
- 152 X. Liu, H. Yang, Y. Liu, X. Gong and H. Huang, Numerical study of clathrin-mediated endocytosis of nanoparticles by cells under tension, *Acta Mech. Sin.*, 2018, **35**(3), 691–701.
- 153 S. Farokhirad, R. P. Bradley and R. Radhakrishnan, Thermodynamic analysis of multivalent binding of functionalized nanoparticles to membrane surface reveals the importance of membrane entropy and nanoparticle entropy in adhesion of flexible nanoparticles, *Soft Matter*, 2019, **15**, 9271–9286.
- 154 D. Bochicchio and L. Monticelli, Chapter Five - The Membrane Bending Modulus in Experiments and



- Simulations: A Puzzling Picture, *Adv. Biomembr. Lipid Self-Assem.*, 2016, **23**, 117–143.
- 155 H. R. Petty, D. G. Hafeman and H. M. McConnell, Disappearance of macrophage surface folds after antibody-dependent phagocytosis, *J. Cell Biol.*, 1981, **89**, 223–229.
- 156 L. V. Mohite, V. A. Juvekar and J. Sahu, Quantification of Polymer–Surface Interaction Using Microcalorimetry, *Ind. Eng. Chem. Res.*, 2019, **58**, 7495–7510.
- 157 D. C. Agrawal, in *Introduction to Nanoscience and Nanomaterials*, World Scientific, 2013, ch. 2: Surfaces.
- 158 H. Amara, J. Nelayah, J. Creuze, A. Chmielewski, D. Alloyeau, C. Ricolleau and B. Legrand, *Is There Really a Size effect on the Surface Energy?*, HAL Open Science, I-03310351, 2021.
- 159 B. Molleman, *Skimming the surface : A surface structural approach to understanding silver ion release from silver nanoparticles*, PhD, Wageningen University, 2019.
- 160 N. Tlotleng, M. A. Vetten, F. K. Keter, A. Skepu, R. Tshikhudo and M. Gulumian, Cytotoxicity, intracellular localization and exocytosis of citrate capped and PEG functionalized gold nanoparticles in human hepatocyte and kidney cells, *Cell Biol. Toxicol.*, 2016, **32**, 305–321.
- 161 D. Li, G. Johanson, C. Emond, U. Carlander, M. Philbert and O. Jolliet, Physiologically based pharmacokinetic modeling of polyethylene glycol-coated polyacrylamide nanoparticles in rats, *Nanotoxicology*, 2014, **8**(Suppl 1), 128–137.
- 162 T. M. Nolte, W. De Cooman, J. P. M. Vink, R. Elst, E. Ryken, A. M. J. Ragas and A. J. Hendriks, Bioconcentration of Organotin Cations during Molting Inhibits Heterocypris incongruens Growth, *Environ. Sci. Technol.*, 2020, **54**, 14288–14301.
- 163 A. J. Hendriks, A. van der Linde, G. Cornelissen and D. T. H. M. Sijm, The power of size. 1. Rate constants and equilibrium ratios for accumulation of organic substances related to octanol-water partition ratio and species weight, *Environ. Toxicol. Chem.*, 2001, **20**, 1399–1420.
- 164 I. A. O'Connor, K. Veltman, M. A. Huijbregts, A. M. Ragas, F. G. Russel and A. J. Hendriks, Including carrier-mediated transport in oral uptake prediction of nutrients and pharmaceuticals in humans, *Environ. Toxicol. Pharmacol.*, 2014, **38**, 938–947.
- 165 M. A. Gronski, J. M. Kinchen, I. J. Juncadella, N. C. Franc and K. S. Ravichandran, An essential role for calcium flux in phagocytes for apoptotic cell engulfment and the anti-inflammatory response, *Cell Death Differ.*, 2009, **16**, 1323–1331.
- 166 J. A. Arnot and F. A. P. C. Gobas, A review of bioconcentration factor (BCF) and bioaccumulation factor (BAF) assessments for organic chemicals in aquatic organisms, *Environ. Rev.*, 2006, **14**, 257–297.
- 167 S. Beulaja Manikandan, R. Manikandan, M. Arumugam and P. Mullainadhan, An overview on human serum lectins, *Heliyon*, 2020, **6**, e04623.
- 168 J. Batson, L. MacCarthy-Morrogh, A. Archer, H. Tanton and C. D. Nobes, EphA receptors regulate prostate cancer cell dissemination through Vav2-RhoA mediated cell-cell repulsion, *Biol. Open*, 2014, **3**, 453–462.
- 169 J. M. Halbleib and W. J. Nelson, Cadherins in development: cell adhesion, sorting, and tissue morphogenesis, *Genes Dev.*, 2006, **20**, 3199–3214.
- 170 C. Y. Loh, J. Y. Chai, T. F. Tang, W. F. Wong, G. Sethi, M. K. Shanmugam, P. P. Chong and C. Y. Looi, The E-Cadherin and N-Cadherin Switch in Epithelial-to-Mesenchymal Transition: Signaling, Therapeutic Implications, and Challenges, *Cells*, 2019, **8**(10), 1118.
- 171 S. M. Furst, P. Sukhai, R. A. McClelland and J. P. Uetrecht, Covalent Binding of Carbamazepine Oxidative Metabolites to Neutrophils, *Drug Metab. Dispos.*, 1995, **23**, 590–594.
- 172 M. W. Panas, Z. Xie, H. N. Panas, M. C. Hoener, E. J. Vallender and G. M. Miller, Trace amine associated receptor 1 signaling in activated lymphocytes, *J. Neuroimmune Pharmacol.*, 2012, **7**, 866–876.
- 173 R. Toy, P. Pradhan, V. Ramesh, N. C. Di Paolo, B. Lash, J. Liu, E. L. Blanchard, C. J. Pinelli, P. J. Santangelo, D. M. Shayakhmetov and K. Roy, Modification of primary amines to higher order amines reduces in vivo hematological and immunotoxicity of cationic nanocarriers through TLR4 and complement pathways, *Biomaterials*, 2019, **225**, 119512.
- 174 S. L. Christian and M. D. Berry, Trace Amine-Associated Receptors as Novel Therapeutic Targets for Immunomodulatory Disorders, *Front. Pharmacol.*, 2018, **9**, 680.
- 175 J. Wu, H. Lin and J. C. Meredith, Poly(ethylene oxide) bionanocomposites reinforced with chitin nanofiber networks, *Polymer*, 2016, **84**, 267–274.
- 176 O. S. Avdeeva, Z. V. Kuropteva, M. K. Pulatova and N. A. Kravchenko, Localization of unpaired electrons in molecules of the substrate inhibitors of lysozyme. II. Oligosaccharides, *Biofizika*, 1977, **22**, 576–581.
- 177 Z. Ma, L. Zhang, Y. Liu, X. Ji, Y. Xu, Q. Wang, Y. Sun, X. Wang, J. Wang, J. Xue and X. Gao, Influential Mechanism of Natural Organic Matters with Calcium Ion on the Anion Exchange Membrane Fouling Behavior via xDLVO Theory, *Membranes*, 2021, **11**(12), 968.
- 178 Q. Li and M. Elimelech, Organic fouling and chemical cleaning of nanofiltration membranes: measurements and mechanisms, *Environ. Sci. Technol.*, 2004, **38**, 4683–4693.
- 179 S. Tokura, S. Nishimura and N. Nishi, Studies on Chitin IX, Specific Binding of Calcium Ion, *Polym. J.*, 1983, **15**, 597–602.
- 180 R. Bos and H. J. Busscher, Role of acid–base interactions on the adhesion of oral streptococci and actinomyces to hexadecane and chloroform—influence of divalent cations and comparison between free energies of partitioning and free energies obtained by extended DLVO analysis, *Colloids Surf., B*, 1999, **14**, 169–177.
- 181 M. Vig and J. P. Kinet, Calcium signaling in immune cells, *Nat. Immunol.*, 2009, **10**, 21–27.



- 182 C. Ràfols, E. Bosch, R. Barbas and R. Prohens, The Ca²⁺-EDTA chelation as standard reaction to validate Isothermal Titration Calorimeter measurements (ITC), *Talanta*, 2016, **154**, 354–359.
- 183 J. O. Joswig, J. Anders, H. Zhang, C. Rademacher and B. G. Keller, The molecular basis for the pH-dependent calcium affinity of the pattern recognition receptor langerin, *J. Biol. Chem.*, 2021, **296**, 100718.
- 184 N. Tiwari, E. R. Blanco, A. Sonzogni, D. Ubieto, H. Wang and M. Calderón, Nanocarriers for Skin Applications: Where Do We Stand?, *Angew. Chem., Int. Ed.*, 2021, **61**, e202107960.
- 185 S. Barua and S. Mitragotri, Challenges associated with Penetration of Nanoparticles across Cell and Tissue Barriers: A Review of Current Status and Future Prospects, *Nano Today*, 2014, **9**, 223–243.
- 186 Y. Huang, N. A. Peppas, Nanoscale Analysis of Mucus-Carrier Interactions for Improved Drug Absorption, in *Nanotechnology in Therapeutics. Current Technology and Applications*, horizon bioscience, Wymondham, 2006.
- 187 C. Liu, X. Jiang, Y. Gan and M. Yu, Engineering nanoparticles to overcome the mucus barrier for drug delivery: Design, evaluation and state-of-the-art, *Med. Drug Discovery*, 2021, **12**, 100110.
- 188 N. A. Peppas, J. Z. Hilt and J. B. Thomas, *Nanotechnology in Therapeutics, Current Technology and Applications*, horizon bioscience, Wymondham, 2006.
- 189 R. Bansil and B. S. Turner, The biology of mucus: Composition, synthesis and organization, *Adv. Drug Delivery Rev.*, 2018, **124**, 3–15.
- 190 S. M. Jafari, *Release and Bioavailability of Nanoencapsulated Food Ingredients*, in Nanoencapsulation in the Food Industry, Charlotte Cockle, 2020, ch. 2.2.1 Mucus layer transport, p. 148.
- 191 L. J. Lawson, V. H. Perry and S. Gordon, Turnover of resident microglia in the normal adult mouse brain, *Neuroscience*, 1992, **48**, 405–415.
- 192 J. Choi, Q. Zheng, H. E. Katz and T. R. Guilarte, Silica-based nanoparticle uptake and cellular response by primary microglia, *Environ. Health Perspect.*, 2010, **118**, 589–595.
- 193 M. L. Kerkeb, F. Gonzhlez-Caballero, B. Jahczukb and T. Biatopiotrowiczb, Components of surface free energy of cholesterol in the presence of bile salts, *Colloids Surf.*, 1992, **62**, 263–272.
- 194 B. Janczuk, M. L. Kerkeb, T. Bialopiotrowicz and F. Gonzalez-Caballero, Surface Free Energy of Cholesterol and Bile Salts from Contact Angle, *J. Colloid Interface Sci.*, 1991, **151**(2), 333–342.
- 195 K. Vijayanand, D. K. Pattanayak, T. R. Ram Mohan and R. Banerjee, Interpreting Blood-Biomaterial Interactions from Surface Free Energy and Work of Adhesion, *Trends Biomater. Artif. Organs*, 2005, **18**(2), 73.
- 196 M. S. Balzer, T. Rohacs and K. Susztak, How Many Cell Types Are in the Kidney and What Do, *Annu. Rev. Physiol.*, 2021, **84**, 507–531.
- 197 A. L. Doiron, B. Clark and K. D. Rinker, Endothelial nanoparticle binding kinetics are matrix and size dependent, *Biotechnol. Bioeng.*, 2011, **108**, 2988–2998.
- 198 J. Ashby, S. Q. Pan and W. W. Zhong, Size and Surface Functionalization of Iron Oxide Nanoparticles Influence the Composition and Dynamic Nature of Their Protein Corona, *ACS Appl. Mater. Interfaces*, 2014, **6**, 15412–15419.
- 199 A. Tomak, S. Cesmeli, B. D. Hanoglu, D. Winkler and C. O. Karakus, Nanoparticle-protein corona complex: understanding multiple interactions between environmental factors, corona formation, and biological activity, *Nanotoxicology*, 2021, **15**, 1331–1357.
- 200 T. Marquardt, T. Brune, K. Luhn, K. P. Zimmer, C. Korner, L. Fabritz, N. van der Werft, J. Vormoor, H. H. Freeze, F. Louwen, B. Biermann, E. Harms, K. von Figura, D. Vestweber and H. G. Koch, Leukocyte adhesion deficiency II syndrome, a generalized defect in fucose metabolism, *J. Pediatr.*, 1999, **134**, 681–688.
- 201 K. C. Stone, R. R. Mercer, P. Gehr, B. Stockstill and J. D. Crapo, Allometric relationships of cell numbers and size in the mammalian lung, *Am. J. Respir. Cell Mol. Biol.*, 1992, **6**, 235–243.
- 202 F. Roussel and J. Dalion, Lectins as markers of endothelial cells: comparative study between human and animal cells, *Lab. Anim.*, 1988, **22**, 135–140.
- 203 D. Wang, Z. Hu, G. Peng and Y. Yin, Surface Energy of Curved Surface Based on Lennard-Jones Potential, *Nanomaterials*, 2021, **11**(3), 686.
- 204 M. I. Setyawati, X. Yuan, J. P. Xie and D. T. Leong, The influence of lysosomal stability of silver nanomaterials on their toxicity to human cells, *Biomaterials*, 2014, **35**, 6707–6715.
- 205 X. W. Ma, Y. Y. Wu, S. B. Jin, Y. Tian, X. N. Zhang, Y. L. Zhao, L. Yu and X. J. Liang, Gold Nanoparticles Induce Autophagosome Accumulation through Size-Dependent Nanoparticle Uptake and Lysosome Impairment, *ACS Nano*, 2011, **5**, 8629–8639.
- 206 J. X. Zhang, X. D. Zhang, G. Liu, D. F. Chang, X. Liang, X. B. Zhu, W. Tao and L. Mei, Intracellular Trafficking Network of Protein Nanocapsules: Endocytosis, Exocytosis and Autophagy, *Theranostics*, 2016, **6**, 2099–2113.
- 207 O. Lunov, T. Syrovets, C. Rucker, K. Tron, G. U. Nienhaus, V. Rasche, V. Mailander, K. Landfester and T. Simmet, Lysosomal degradation of the carboxydextran shell of coated superparamagnetic iron oxide nanoparticles and the fate of professional phagocytes, *Biomaterials*, 2010, **31**, 9015–9022.
- 208 R. Gupta, Y. Badhe, S. Mitragotri and B. Rai, Permeation of nanoparticles across the intestinal lipid membrane: dependence on shape and surface chemistry studied through molecular simulations, *Nanoscale*, 2020, **12**, 6318–6333.
- 209 J. Dumková, T. Smutná, L. Vrlíková, P. Le Coustumer, Z. Večeřa, B. Dočekal, P. Mikuška, L. Čapka, P. Fictum, A. Hampl and M. Buchtová, Sub-chronic inhalation of lead oxide nanoparticles revealed their broad distribution and tissue-specific subcellular localization in target organs, *Part. Fibre Toxicol.*, 2017, **14**, 55.



- 210 W. C. Chou, Y. H. Cheng, J. E. Riviere, N. A. Monteiro-Riviere, W. G. Kreyling and Z. Lin, Development of a multi-route physiologically based pharmacokinetic (PBPK) model for nanomaterials: a comparison between a traditional versus a new route-specific approach using gold nanoparticles in rats, *Part. Fibre Toxicol.*, 2022, **19**, 47.
- 211 N. Hoshyar, S. Gray, H. Han and G. Bao, The effect of nanoparticle size on in vivo pharmacokinetics and cellular interaction, *Nanomedicine*, 2016, **11**, 673–692.
- 212 E. Yaghini, E. Tacconi, A. Pilling, P. Rahman, J. Broughton, I. Naasani, M. R. S. Keshtgar, A. J. MacRobert and O. Della Pasqua, Population pharmacokinetic modelling of indium-based quantum dot nanoparticles: preclinical in vivo studies, *Eur. J. Pharm. Sci.*, 2021, **157**, 105639.
- 213 L. Geraets, A. G. Oomen, P. Krystek, N. R. Jacobsen, H. Wallin, M. Laurentie, H. W. Verharen, E. F. Brandon and W. H. de Jong, Tissue distribution and elimination after oral and intravenous administration of different titanium dioxide nanoparticles in rats, *Part. Fibre Toxicol.*, 2014, **11**, 30.
- 214 Y. Zheng and B. Nowack, Meta-analysis of Bioaccumulation Data for Nondissolvable Engineered Nanomaterials in Freshwater Aquatic Organisms, *Environ. Toxicol. Chem.*, 2022, **41**, 1202–1214.
- 215 X. R. Xia, N. A. Monteiro-Riviere and J. E. Riviere, An index for characterization of nanomaterials in biological systems, *Nat. Nanotechnol.*, 2010, **5**, 671–675.
- 216 L. Ponsonnet, K. Reybier, N. Jaffrezic, V. Comte, C. Lagneau, M. Lissac and C. Martelet, Relationship between surface properties (roughness, wettability) of titanium and titanium alloys and cell behaviour, *Mater. Sci. Eng., C*, 2003, **23**, 551–560.
- 217 R. Bos, H. J. Busscher, G. I. Geertsema-Doornbusch and H. C. Van Der Mei, Acid-base interactions in microbial adhesion to hexadecane and chloroform, in *2nd International Symposium on Acid-Base Interactions - Relevance to Adhesion Science and Technology*, Newark, NJ, 1998, pp. 513–524.
- 218 Y. Xiao and M. R. Wiesner, Characterization of surface hydrophobicity of engineered nanoparticles, *J. Hazard. Mater.*, 2012, **215**, 146–151.
- 219 A. Valsesia, C. Desmet, I. Ojea-Jiménez, A. Oddo, R. Capomaccio, F. Rossi and P. Colpo, Direct quantification of nanoparticle surface hydrophobicity, *Commun. Chem.*, 2018, **1**, 53.
- 220 J. A. J. Meesters, A. A. Koelmans, J. T. K. Quik, A. J. Hendriks and D. van de Meent, Multimedia Modeling of Engineered Nanoparticles with SimpleBox4nano: Model Definition and Evaluation, *Environ. Sci. Technol.*, 2014, **48**, 5726–5736.
- 221 J. D. Crapo, B. E. Barry, P. Gehr, M. Bachofen and E. R. Weibel, Cell number and cell characteristics of the normal human lung, *Am. Rev. Respir. Dis.*, 1982, **126**, 332–337.
- 222 L. M. Sweeney, L. MacCalman, L. T. Haber, E. D. Kuempel and C. L. Tran, Bayesian evaluation of a physiologically-based pharmacokinetic (PBPK) model of long-term kinetics of metal nanoparticles in rats, *Regul. Toxicol. Pharmacol.*, 2015, **73**, 151–163.
- 223 Z. Lin, N. A. Monteiro-Riviere and J. E. Riviere, A physiologically based pharmacokinetic model for polyethylene glycol-coated gold nanoparticles of different sizes in adult mice, *Nanotoxicology*, 2016, **10**, 162–172.

